Chemical freeze-out conditions and fluctuations of conserved charges in heavy-ion collisions within a quantum van der Waals model

R. V. Poberezhnyuk,[1,2] V. Vovchenko,[3,2] A. Motornenko,[3,2] M. I. Gorenstein,[1,2] and H. Stöcker[3,2,4]

[1]*Bogolyubov Institute for Theoretical Physics, 03680 Kiev, Ukraine*

[2]*Frankfurt Institute for Advanced Studies, Giersch Science Center, D-60438 Frankfurt am Main, Germany*

[3]*Institut für Theoretische Physik, Goethe Universität Frankfurt, D-60438 Frankfurt am Main, Germany*

[4]*GSI Helmholtzzentrum für Schwerionenforschung GmbH, D-64291 Darmstadt, Germany*

(Received 18 June 2019; revised manuscript received 26 August 2019; published 12 November 2019)

The chemical freeze-out parameters in central nucleus-nucleus collisions are extracted consistently from hadron-yield data within the quantum van der Waals (QvdW) hadron resonance gas model. The beam energy dependencies for skewness and kurtosis of net baryon, net electric, and net strangeness charges are predicted. The QvdW interactions in asymmetric matter, $Q/B \neq 0.5$, between (anti)baryons yield a noncongruent liquid-gas phase transition, together with a nuclear critical point (CP) with critical temperature of $T_c = 19.5$ MeV. The nuclear CP shows that the collision energy dependence of the skewness and the kurtosis both deviate significantly from the ideal hadron resonance gas baseline predictions even far away, in the (T, μ_B) plane, from the CP. These predictions can readily be tested by the STAR and NA61/SHINE Collaborations at the RHIC BNL and the SPS CERN, respectively, and by HADES at GSI. The results presented here offer a broad opportunity for the search for signals of phase transition in dense hadronic matter at the future NICA and FAIR high-intensity facilities.

DOI: 10.1103/PhysRevC.100.054904

I. INTRODUCTION

The structure of the phase diagram of strongly interacting matter is one of the most important and still open topics in nuclear and particle physics to date. The known phenomenology of the physics of strong interactions suggests both short-range repulsion and intermediate-range attraction between nucleons in proximity of nuclear saturation density $n_0 = 0.16$ fm^{-3}. This yields a first-order liquid-gas phase transition (LGPT) from a dilute (gaseous) to a dense (liquid) phase of nuclear matter, which smooths out in the nuclear critical point (CP). In contrast to the hypothetical deconfinement-related CP, the existence of the LGPT and the nuclear CP is better established [1–15]; see Ref. [16] for a review.

Theoretical arguments suggest the enhancement of certain fluctuations of conserved quantities in the critical region [17–22]; namely, the fluctuation of the conserved charges that are related to the so-called order parameter. The signals of the CP in the scaled variance of the charge fluctuations fade out rather quickly when moving away from the CP [23,24]. On the other hand, the CP signals in fluctuation measures which are related to the higher-order moments of charge distributions; namely, skewness and kurtosis of charge fluctuations, can be seen even far away from the location of the CP on the phase diagram [25–27]. Thus, the observed large deviations of the higher-order charge fluctuations from the ideal hadron resonance gas (IHRG) baseline can be taken as a signal for the existence of a CP.

Here we study this issue by employing the quantum van der Waals hadron resonance gas (QvdW-HRG) model, which is the extension of the classical vdW model: The QvdW model was recently generalized to include the grand canonical ensemble (GCE) [28], the effects of relativity and quantum statistics [25], and the full known spectrum of hadrons and resonances [27]. The QvdW-HRG model is a minimal interaction extension of the IHRG model. It takes into account both attractive and repulsive interactions between only baryons and between only antibaryons. These interactions yield the LGPT and the nuclear CP within the model [25]. The model includes only two parameters, which are fixed by the properties of the nuclear ground state.

The QvdW-HRG at low temperatures is reduced to normal nuclear matter, described by the QvdW model; see Refs. [23,25,26,28–30]. The results for symmetric nuclear matter are similar to the Walecka model results [31]. The QvdW model was applied to describe asymmetric nuclear matter and its noncongruent LGPT in Ref. [24].

The skewness and the kurtosis of baryonic charge fluctuations were calculated within the QvdW-HRG model for central nucleus-nucleus $(A + A)$ collisions along the chemical freeze-out line in Ref. [26]. The present paper extends these results in two directions. First, the chemical freeze-out line is derived consistently for central $A + A$ collisions within the QvdW-HRG model. Second, both the baryonic and electric charge fluctuations are calculated in T-μ_B plane and along the freeze-out line. The electric charge is a more

convenient quantity for experimental measurement, compared with baryonic charge because it does not require the detection of the dominant electrically neutral baryons. The THERMALFIST [32] package is used for the calculations within the QvdW-HRG model.

The paper is organized as follows: Section II briefly describes the QvdW-HRG model. Section III discusses the noncongruent LGPT in asymmetric nuclear matter within the QvdW-HRG model and presents chemical freeze-out lines obtained within the QvdW-HRG and IHRG models. Section IV presents the QvdW-HRG and IHRG results on the skewness and the kurtosis of charge fluctuations as functions of the collision energy and in the coordinates of baryochemical potential and temperature. A summary closes the article in Sec. V.

II. THE QUANTUM VAN DER WAALS-HADRON RESONANCE GAS MODEL

The total baryon (B), electric (Q), and strangeness (S) charges of the hot, dense, hadronic system in the GCE are regulated by the corresponding chemical potentials, μ_B, μ_Q, and μ_S. The chemical potential of the jth type hadron is $\mu_j = b_j\mu_B + s_j\mu_S + q_j\mu_Q$, where b_j, s_j, and q_j are, respectively, the baryonic number, the strangeness, and the electric charge of the hadron of j type. The QvdW model yields the total pressure of the system as a sum of the partial pressures of baryons, antibaryons, and mesons [27]:

$$p(T,\mu) = p_B + p_{\bar{B}} + p_M. \tag{1}$$

The partial pressure of the baryons is given as

$$p_B(T,\mu) = \sum_{j\in B} p_j^{\rm id}\left(T,\mu_j^{B*}\right) - an_B^2\,. \tag{2}$$

Here T is the temperature, $p_j^{\rm id}$ is the ideal Fermi-Dirac pressure of the baryons of j type, and μ_j^{B*} and n_B are, respectively, the shifted baryonic chemical potential of baryons of j type and the total density of all baryons:

$$\mu_j^{B*} = \mu_j - b\,p_B - a\,b\,n_B^2 + 2\,a\,n_B, \tag{3}$$

$$n_B = \left[\frac{\partial p_B}{\partial \mu_B}\right]_T = \sum_{j\in B} n_j = (1-bn_B)\sum_{j\in B} n_j^{\rm id}\left(T,\mu_j^{B*}\right). \tag{4}$$

The corresponding expressions for $p_{\bar{B}}$, $\mu_j^{\bar{B}*}$, and $n_{\bar{B}}$ of the antibaryons are analogous to Eqs. (2)–(4). The QvdW interactions are assumed to exist separately between all pairs of baryons and between all pairs of antibaryons, where the same parameters are used for all (anti-)baryons as for nucleons: $a = 329$ MeV fm^3 and $b = 3.42$ fm^3 [27]. These parameters a and b were obtained in Ref. [23] by fitting the saturation density, $n^{\rm GS} = 0.16$ fm^{-3}, and binding energy, $E_b^{\rm GS} = -16$ MeV, of the ground state of symmetric nuclear matter. Possible QvdW interactions for baryon-antibaryon, meson-meson, and meson-(anti-)baryon pairs are neglected. The partial pressure of all mesons is taken as a sum of the ideal Bose-Einstein gas pressures. The summation in Eqs. (2)–(4) is performed over all hadrons and resonances listed in the Particle Data Tables [33] and which have a confirmed status there.

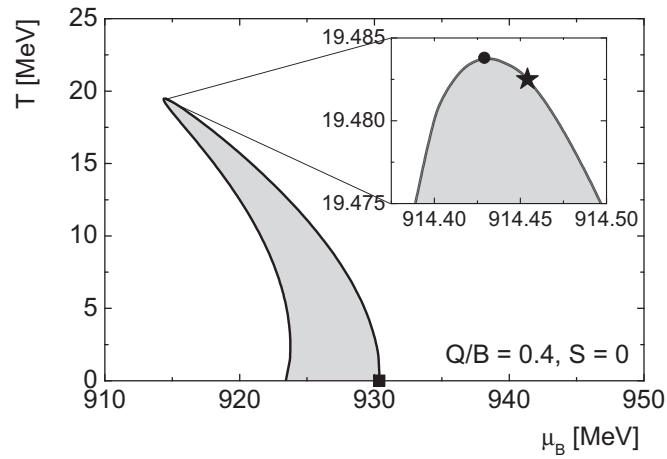

FIG. 1. Liquid-gas phase transition for asymmetric nuclear matter with an asymmetry parameter of $Q/B = 0.4$ in (μ_B, T) coordinates. The shaded area represents the mixed phase. The ground state is denoted by a square. The inset shows a zoomed-in picture of the region around the critical point. The critical point and the temperature endpoint are shown by the star and the circle, respectively.

III. PHASE TRANSITION AND CHEMICAL FREEZE-OUT

The LGPT in the QvdW-HRG model is due to an interplay of the repulsive and the attractive interactions. The mixed phase boundary and the location of the CP in asymmetric nuclear matter are found from the Gibbs equilibrium condition [24]. The QvdW-HRG model with $Q/B = 0.4$ exhibits the CP at $\mu_B^c = 914.5$ MeV, $T_c = 19.48$ MeV. The LGPT region in the (μ_B, T) coordinates is shown in Fig. 1.

We fix the ratio of the electric-to-baryon charge (asymmetry parameter): $Q/B = 0.4$. This approximately corresponds to the isospin asymmetry in heavy nuclei like lead (Pb) or gold (Au). Note that isospin asymmetry alters qualitatively the properties of the PT, rendering it as being a "noncongruent" PT. As a result, the mixed phase in (μ_B, T) coordinates cannot be presented by a line, but is rather a region of finite width. Moreover, for a noncongruent PT, the location of the CP differs from the location of the temperature endpoint (TEP), the point with the maximum temperature at which the phase coexistence is possible. The inset in Fig. 1 zooms in on the region of the CP. The star and the circle represent the CP and the TEP, respectively, see Refs. [24,34] for details.

The particle number fluctuations in $A + A$ collisions are calculated within statistical models at different collision energies by using the chemical freeze-out values of the temperature and baryochemical potential. In the present paper we use the data on mean hadron multiplicities in various experiments at SchwerIonen-Synchrotron (SIS), Alternating Gradient Synchrotron (AGS), Super Proton Synchrotron (SPS), and Large Hadron Collider (LHC) to determine the chemical freeze-out values for the QvdW-HRG model.

The GCE can be used for all datasets considered, except for the lowest energies at the SIS. The exact net strangeness conservation is enforced for the SIS data, i.e., the calculations are done for these low-energy Au + Au collisions within the strangeness canonical ensemble (SCE) [54,55].

TABLE I. The results of the hadron chemical freeze-out parameters fits for the IHRG and the QvdW model.

$\sqrt{s_{NN}}$		IHRG				QvdW-HRG			
[GeV]	Refs.	μ_B [MeV]	T [MeV]	V [fm^3]	γ_s	μ_B [MeV]	T [MeV]	V [fm^3]	γ_s
2760	[35–38]	1.4 ± 9.7	153 ± 3	4741 ± 540	1.11 ± 0.03	1.5 ± 10.9	156 ± 5	4148 ± 613	1.10 ± 0.03
17.3	[39–46]	246 ± 10	150 ± 3	4885 ± 522	0.87 ± 0.03	314 ± 39	160 ± 7	3503 ± 543	0.81 ± 0.04
12.3	[39–43]	289 ± 14	151 ± 5	3552 ± 447	0.72 ± 0.04	356 ± 48	153 ± 9	3474 ± 474	0.69 ± 0.04
8.8	[39–43]	372 ± 12	145 ± 4	2657 ± 304	0.80 ± 0.04	443 ± 46	143 ± 7	3210 ± 345	0.78 ± 0.04
7.7	[40–42,47]	415 ± 11	143 ± 4	2210 ± 268	0.84 ± 0.05	491 ± 57	138 ± 8	3093 ± 369	0.80 ± 0.05
6.3	[40–42,47]	469 ± 12	138 ± 7	1935 ± 404	0.82 ± 0.05	566 ± 106	131 ± 10	2829 ± 654	0.83 ± 0.05
4.9	[48–51]	569 ± 16	120 ± 4	2905 ± 695	0.70 ± 0.08	634 ± 81	119 ± 8	2896 ± 815	0.70 ± 0.08
2.3	[52,53]	808 ± 25	48.3 ± 2			802 ± 23	48.3 ± 2		

Finite-resonance widths are treated in the present paper in the framework of an energy-independent Breit-Wigner scheme [56]. Note that the energy dependent Breit-Wigner scheme leads to a better description of hadron yields at the LHC [56]. Another possibility is to neglect the finite widths of resonances altogether. Here we stick to the energy-independent Breit-Wigner scheme so as to preserve consistency with our earlier works regarding the chemical freeze-out conditions in the IHRG model [57] or thermodynamic properties of the QvdW-HRG model [27]. We did verify that differences in the extracted freeze-out parameters obtained within these different schemes are small, with a possible exception of the strangeness saturation factor γ_S. A detailed study of finite-resonance-width effects on hadron yields for intermediate collision energies will be presented elsewhere.

The fitted freeze-out parameters are μ_B, T, volume of the system V, and the strangeness under-saturation parameter γ_S (see Ref. [58]). The corresponding IHRG and QvdW-HRG fit results for μ_B, T, V, and γ_s are presented in Table I. In the SCE for the SIS data we set the strangeness correlation volume equal to the volume of the system, i.e., $V_c = V$. The extracted values of the chemical freeze-out parameters, T and μ_B, are plotted for all energies in Figs. 2(a) and 2(b) for the IHRG and QvdW-HRG models, respectively. The values of γ_s for both the IHRG and QvdW-HRG models are plotted in Fig. 3(a). The Au + Au data at SIS allow us to extract both the temperature and the baryochemical potential. They are shown in Figs. 2(a) and 2(b). The parameter γ_S, however, cannot be reliably determined (see Ref. [57]). Hence, γ_S is not shown in Fig. 3(a) at SIS. We define the uncertainties of the extracted μ_B, T, and γ_s values following the procedures given in Ref. [59], by multiplying the uncertainties inferred from the $\chi^2 = \chi^2_{\rm min} + 1$ contours by a factor $(\chi^2_{\rm min}/{\rm dof})$ [33], where "dof" means "degrees of freedom."

The higher temperatures and larger uncertainties of T and μ_B values in the QvdW-HRG model are mainly due to the excluded volume interactions of (anti-)baryons which is incorporated in this model. Such an effect has been reported before for different variants of the excluded volume HRG model [60,61]. Moreover, an appearance of peculiar two-minima structures in χ^2 are possible when deviations from the IHRG model picture are considered [62], although physics interpretation of the second minimum at higher temperatures is challenging. For the QvdW-HRG model used here we do

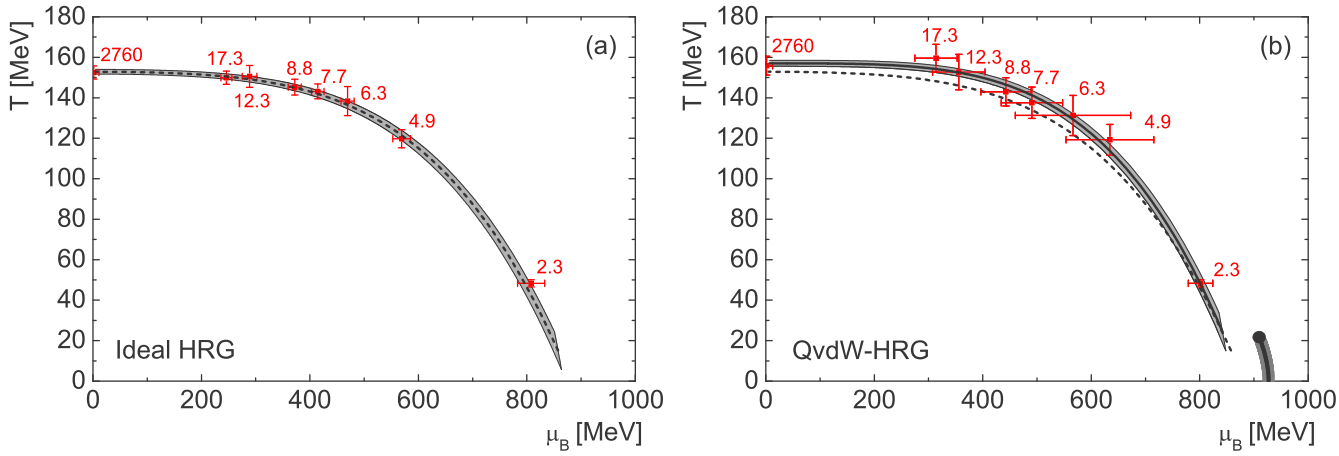

FIG. 2. Freeze-out lines according to Eq. (5) are shown in the (μ_B, T) coordinates plane all the way from collision energies $\sqrt{s_{NN}} =$ 1.9 GeV to 2.8 TeV for (a) the Ideal-HRG and (b) the QvdW-HRG model. The shaded areas along the curves represent the uncertainties. The Ideal-HRG freeze-out line is represented in panel (b) by the dashed line for comparison with the QvdW-HRG curve. The numbers on the freeze-out line give the respective center-of-mass energy, $\sqrt{s_{NN}}$, in GeV. The first-order phase transition region and the nuclear critical point are also shown in panel (b) by the dark curve and the dot, respectively.

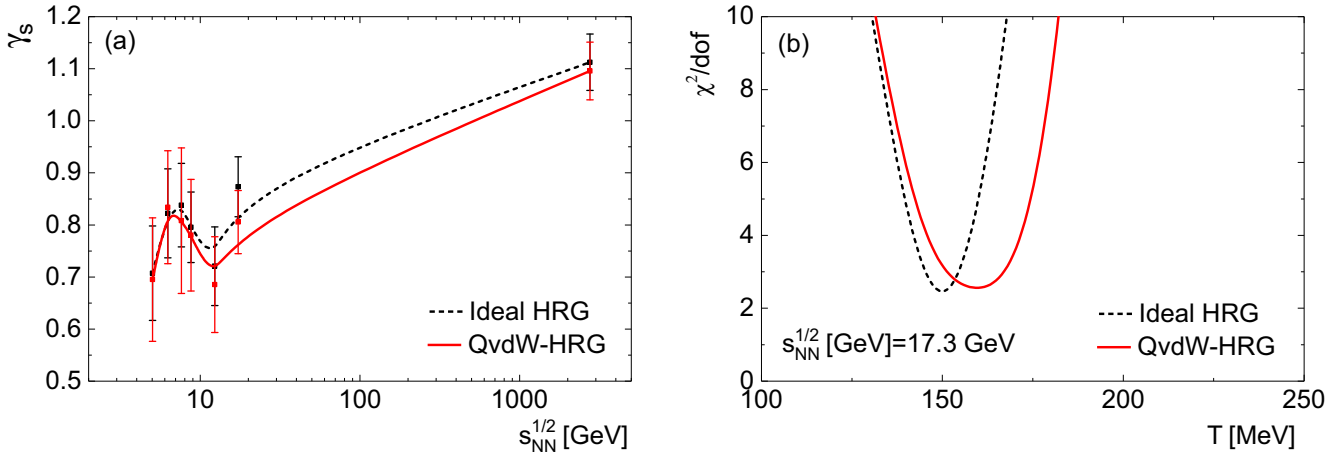

FIG. 3. (a) γ_S is shown along the chemical freeze-out line as a function of collision energy. (b) The temperature dependence of χ^2/dof of the fits to NA61/SHINE data at $\sqrt{s_{NN}} = 17.3$ GeV using the IHRG (black dashed curves) and QvdW-HRG (red solid curves) model, respectively. Note the higher temperature, $\Delta T \approx 10$ MeV, obtained from the QvdW-HRG fit.

observe a second minimum in the χ^2 temperature profile of the ALICE data fit at $T \sim 200$ MeV, but we do not observe any two-minima structures for all other data sets (SPS and SIS) used in our analysis. Figure 3(b) depicts the temperature profile of χ^2/dof of the fit to the NA49 data at top SPS energy ($\sqrt{s_{NN}} = 17.3$ GeV), the picture for all other energies (except LHC) is similar. This figure illustrates the broadening of the χ^2 profile when QvdW interactions between baryons are switched on.

We adopt a simple thermodynamic parametrization of the chemical freeze-out line,

$$T = a_1 - a_2\mu_B^2 - a_3\mu_B^4, \quad \mu_B = \frac{b_1}{1 + b_2\sqrt{s_{NN}}}, \qquad (5)$$

used previously in Ref. [63]. Here we use it to parametrize the extracted T and μ_B values. The five newly fit parameters in Eq. (5), a_1, a_2, a_3, b_1, b_2, are presented in Table II for both the IHRG and QvdW-HRG models. Note that the QvdW-HRG parameters a_2, a_3, b_1 differ by about 20% from the IHRG fits, but that the b_2 value of the IHRG fit exceeds the QvdW-HRG value by 70%. The parametrization (5) extrapolates the freeze-out line from the $\mu_B \approx 0$ region at the highest collision energies down to the nuclear-matter region of the phase diagram at the lowest collision energies. The chemical freeze-out line close to the region of the nuclear liquid-gas transition was previously considered in Refs. [64,65] in the context of light-cluster formation.

Figures 4(a) and 4(b) present, respectively, the net baryon density n_B and the entropy per baryon, s/n_B, along the chemical freeze-out line as a function of collision energy for the two models. At low $\sqrt{s_{NN}}$ in both QvdW-HRG and IHRG models freeze-out takes place in a diluted region. At the lowest considered energy of $\sqrt{s_{NN}} = 1.9$ GeV freeze-out in both models takes place at baryon density of $n_B = 2.17 \times 10^{-4}$ fm^{-3}. The net baryon density exhibits a maximum as a function of collision energy, as first noted in Ref. [66] for the IHRG model. Within the QvdW-HRG model this maximum is lower in comparison with the IHRG model, which is due to the excluded volume repulsion between (anti-)baryons (see also Ref. [67]). The behavior of the entropy per baryon is very similar for both models, indicating that s/n_B is a robust observable that depends little on the details of the HRG model [61].

IV. FLUCTUATIONS

The skewness $S\sigma$ and the kurtosis $\kappa\sigma^2$ of the baryonic, $ch = B$, and the electric, $ch = Q$, charge fluctuations are expressed as ratios of normalized cumulants (susceptibilities):

$$S\sigma[\mathrm{ch}] = \frac{\chi_3^{\mathrm{ch}}}{\chi_2^{\mathrm{ch}}}, \quad \kappa\sigma^2[\mathrm{ch}] = \frac{\chi_4^{\mathrm{ch}}}{\chi_2^{\mathrm{ch}}}. \qquad (6)$$

Susceptibilities χ_i^{ch} are calculated in the GCE from the scaled total pressure by taking the derivatives with respect to the corresponding powers of the chemical potentials over the temperature:

$$\chi_n^{\mathrm{ch}} = \frac{\partial^n(p/T^4)}{\partial(\mu_{\mathrm{ch}}/T)^n}. \qquad (7)$$

Figures 5 and 6 show the skewness and the kurtosis of, respectively, the baryonic and the electric charge fluctuations in the (μ_B, T) coordinate plane as calculated in the IHRG

TABLE II. The freeze-out line parameters [see Eq. (5)] for the Ideal-HRG and the QvdW-HRG models.

	a_1 [GeV]	a_2 [GeV^{-1}]	a_3 [GeV^{-3}]	b_1 [GeV]	b_2 [GeV^{-1}]
IHRG	0.152 ± 0.001	0.026 ± 0.003	0.219 ± 0.004	1.310 ± 0.006	0.278 ± 0.003
QvdW	0.157 ± 0.002	0.0032 ± 0.0027	0.259 ± 0.004	1.094 ± 0.004	0.157 ± 0.002

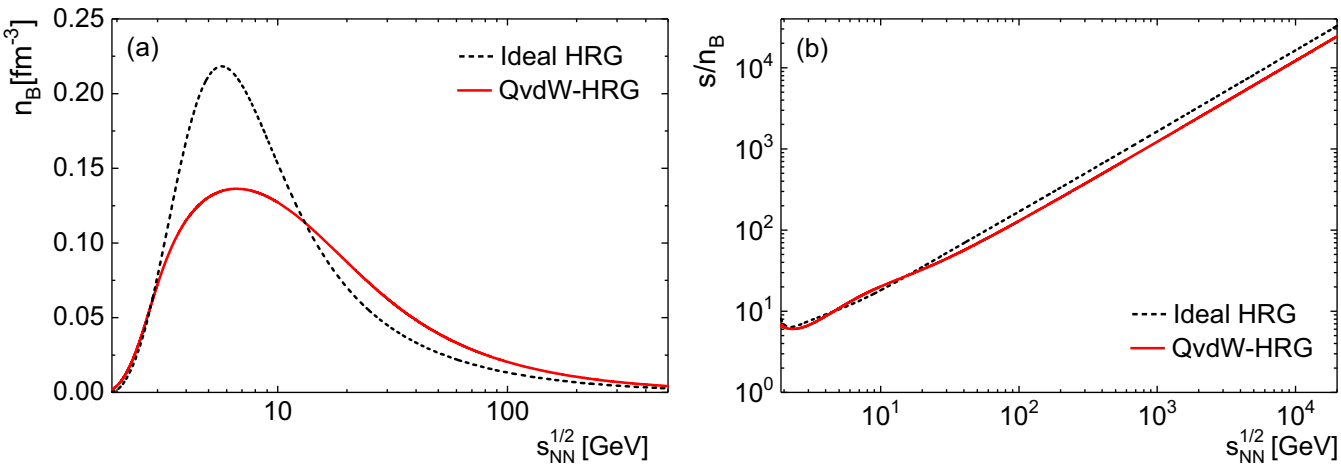

FIG. 4. (a) Net baryon density and (b) entropy per baryon are shown along the chemical freeze-out line as a function of collision energy.

and the QvdW-HRG models. White coloring corresponds to $S\sigma = \kappa\sigma^2 = 1$. The third-order susceptibility is antisymmetric with respect to hadrons and antihadrons, $\chi_3^{\rm ch} = \chi_3^h - \chi_3^{\bar{h}}$. At $\mu_B = 0$ the numbers of hadrons and antihadrons are equal. Therefore, at $\mu_B = 0$ the skewness of both charge fluctuations in both models equals zero, $S\sigma = 0$. In contrast, the fourth-order susceptibility is symmetric with respect to hadrons and antihadrons, $\chi_4^{\rm ch} = \chi_4^h + \chi_4^{\bar{h}}$. Therefore, the values for χ_4 of

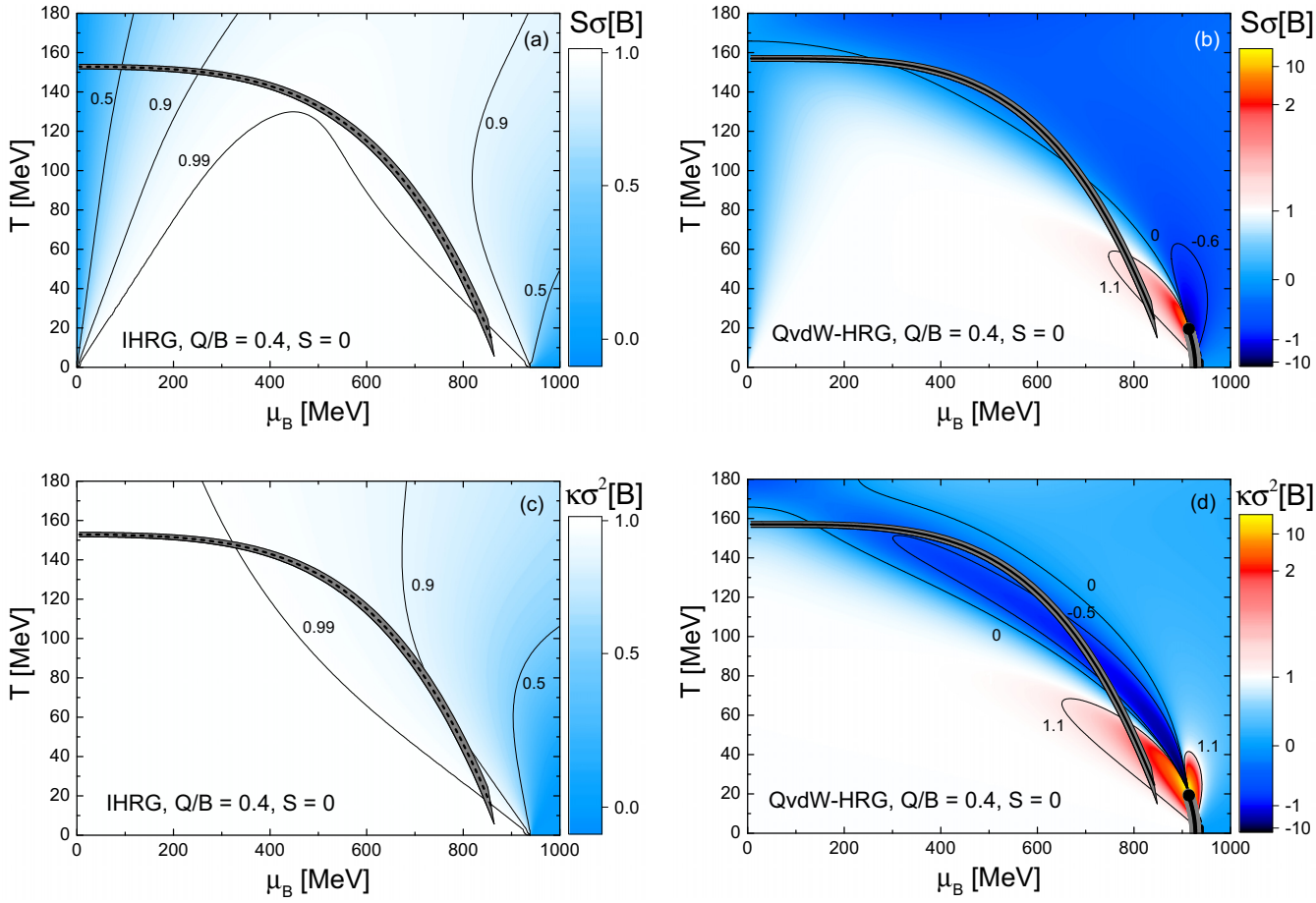

FIG. 5. (a), (b) Skewness $S\sigma$ and (c), (d) kurtosis $\kappa\sigma^2$ of baryonic charge fluctuations in (μ_B, T) coordinates obtained in (a), (c) the IHRG model and (b), (d) the QvdW-HRG model for strongly interacting matter with asymmetry parameter $Q/B = 0.4$. The freeze-out lines for both models are also shown. Note the large differences between the two model predictions for both skewness and kurtosis.

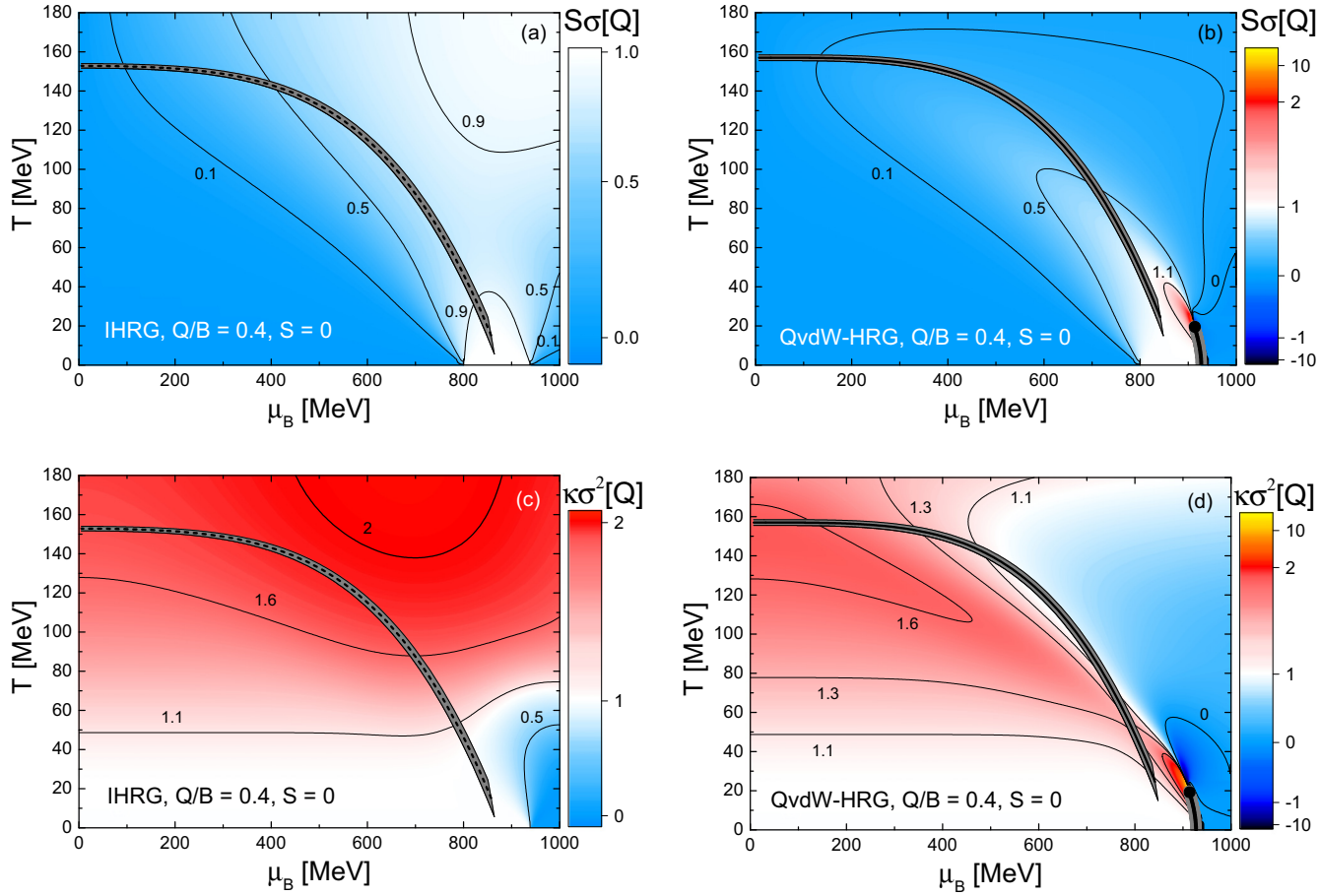

FIG. 6. The same as in Fig. 5 but for electric charge fluctuations.

particle and antiparticle fluctuations do not cancel each other at $\mu_B = 0$. At high temperatures, the contribution of the pions, which are Bose particles, to χ_4^Q is substantial. This contributes to the large positive values of $\kappa\sigma^2[Q] \approx 1.6$ at high temperatures.

The fluctuations exhibit a singular behavior at the CP: both the skewness and the kurtosis of charge fluctuations can approach the values $+\infty$, $-\infty$, or 0, depending on the path with which the CP is approached in the phase diagram. The strong influence of the CP on the higher moments of the distributions is apparent even far away from the CP. This is particularly true along the freeze-out lines.

We have checked that the strangeness suppression effect due to $\gamma_s < 1$ is rather small in the skewness and kurtosis of the net strangeness fluctuations. Therefore, in calculations of charge fluctuations, γ_s is fixed to unity and the GCE is used. Figure 7 shows the skewness and the kurtosis of the charge fluctuations as functions of the center-of-mass energy $\sqrt{s_{NN}}$ as calculated in the IHRG and QvdW-HRG models, along the corresponding fitted chemical freeze-out lines (5). The nontrivial behavior of higher-order fluctuations measures superimposed on the shape of the freeze-out line leads to the complex, nonmonotonic behavior of these quantities as functions of the collision energy. A pure asymmetric nuclear matter (the only constituents are nucleons) models both $S\sigma[B]$ and $\kappa\sigma^2[B]$ rather well at moderate and low collision energies, $\sqrt{s_{NN}} \lesssim 2.4$ GeV. This energy corresponds to temperatures of $T \lesssim 60$ MeV. However, for a quantitative description of the $S\sigma[Q]$ and the $\kappa\sigma^2[Q]$ values, this approximation is not good enough because, even at the lower energies, the contribution of the direct pions to the electric charge is quite substantial. Accounting for both nucleons and direct pions does allow for a reasonable description of the skewness of the electric charge fluctuations up to GSI energies, $\sqrt{s_{NN}} \lesssim 2.4$ GeV. The deviations of the strangeness fluctuations at the intermediate beam energies from the IHRG baseline are mostly due to the contributions of strange baryons, mainly Λ and Σ, which take part in the QvdW interactions.

The results of the QvdW-HRG model for $\kappa\sigma^2[Q]$ and $\kappa\sigma^2[S]$ at high collision energies are close to the IHRG baseline. This is due to the large contributions of pions and kaons, respectively, which are treated as noninteracting particles within QvdW-HRG approach. In contrast, $\kappa\sigma^2[B]$ at high energies substantially deviates from the IHRG baseline due to interactions between (anti-)baryons.

Figures 5 and 6 demonstrate that the values of high-order charge fluctuations are highly sensitive to the location on the phase diagram. This sensitivity is strongest in proximity to the CP. In the QvdW-HRG model the fluctuations of the conserved charges in the system of nucleons at small temperatures are rather different in the dilute gaseous and dense liquid phases of interacting nucleons. Within the QvdW-HRG

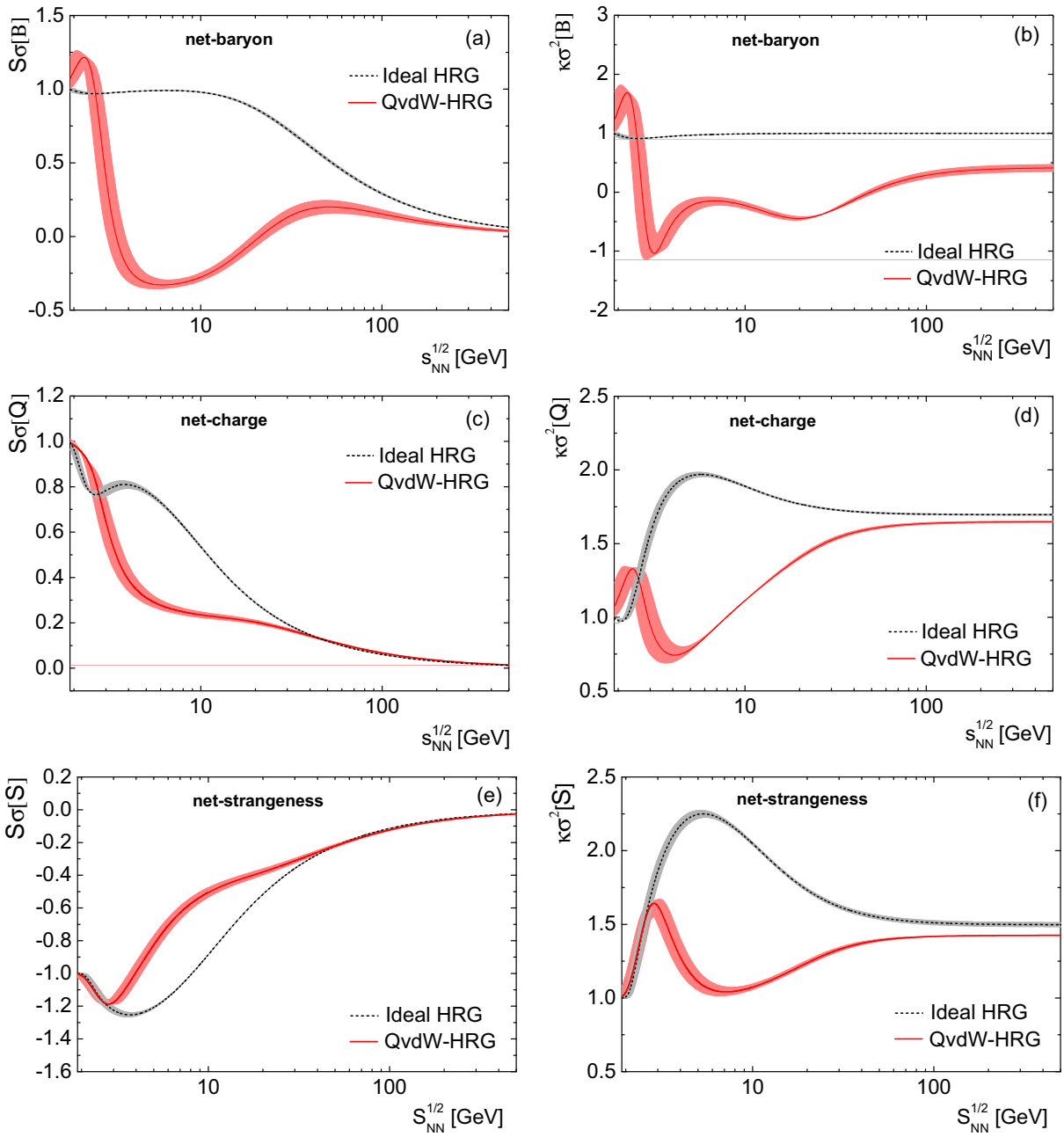

FIG. 7. Skewness (left-hand side) and kurtosis (right-hand side) of (a), (b) baryonic; (c), (d) electric; and (e), (f) strangeness charge fluctuations within the IHRG (dashed black curves) and QvdW-HRG (solid red curves) models, along the respective freeze-out lines of the models. The shaded areas along the curves represent the uncertainties of the predicted results due to the uncertainties of the fitted freeze-out line parameters. Note that the predicted large differences of the fluctuation measures at BES II, GSI, and FAIR energies, fully accessible experimentally to date.

model, the chemical freeze-out at the lowest $\sqrt{s_{NN}}$ takes place in the gaseous phase where the effects of the interactions are rather small. Thus, strong deviations of the QvdW-HRG model fluctuations from the IHRG baseline appear mostly at intermediate beam energies where the baryonic density is the highest; see Fig. 4(a). Note that, at present, there is a lack of hadron multiplicity data in nucleus-nucleus collisions at low collision energies. Our analysis shows a strong sensitivity of high-order charge fluctuations to the position of the chemical freeze-out line relative to the nuclear CP. More data for hadron multiplicities in nucleus-nucleus reactions at low collision energies are required to clarify the production of new hadrons as well as the final fractions of the light and intermediate nuclear fragments.

A quantitative comparison with the data in heavy-ion collisions requires the appropriately chosen acceptance region. This region is defined by the cuts in rapidity, transverse momentum, azimuthal angle, and other experimental limitations of measurements. For event-by-event measurements in nucleus-nucleus reactions the *required acceptance* region

should satisfy certain requirements. It should be a small part of the whole phase space; thus, the global charge conservation effects can be disregarded, and the statistical treatment within the grand canonical ensemble can be applied. On the other hand, this acceptance region should be large enough to capture the relevant physics.

To reduce the volume fluctuation effects, the most-central collisions must be selected [68]. Another way to reduce the volume fluctuation effects is to use the so-called strongly intensive quantities [69] as the fluctuation measures. A detailed analysis of the required acceptance and volume fluctuation corrections is, however, outside the scope of the present paper and will be a subject of future research.

The baryon number fluctuations are calculated in the present paper with the assumption that all baryons are experimentally detectable. This is not the case in reality. Therefore, a binomial acceptance procedure (see Refs. [21,26,70]) is usually applied to account for this inability of the event-by-event measurements of (anti)neutron numbers. This procedure leads to an essential decrease of the observable baryon number fluctuations. In contrast with the baryon number, nearly all electric charges can be experimentally detected. Thus, our results obtained for electric charge fluctuations are more suitable for a comparison with the experimental data.

Finally, an analysis of experimental data should be complemented with dynamical model simulations of heavy-ion collisions, where the effects of baryon-baryon interactions studied here are incorporated. The dynamical models can naturally incorporate the effects related to baryon number conservation and acceptance. Some recent developments in this direction using transport models can be found in Refs. [71,72].

Note that the predicted large differences of the fluctuation measures at the high baryon density correspond to the center-of-mass energy regime from 3 to 30 GeV, which is readily accessible to the Beam Energy Scan II run at Brookhaven National Laboratory, and at the Helmholtzzentrum für Schwerionenforschung (GSI) HADES detector, as well as the Compressed Baryonic Matter (CBM) detector at Facility for Antiproton and Ion Research (FAIR) and the Multi Purpose Detector (MPD) at NICA in Dubna.

V. SUMMARY

The quantum van der Waals hadron resonance gas model has been applied to study chemical freeze-out properties in heavy-ion collisions as well as the higher-order fluctuations of net baryon and net charge numbers. The extracted chemical freeze-out parameters exhibit larger uncertainties as compared with the ideal hadron resonance gas model. Similar to the IHRG model, the dependence of $T_{\rm ch}$ on $\mu_B^{\rm ch}$ in the QvdW-HRG model can be parametrized as a quartic polynomial in $\mu_B^{\rm ch}$, with parameters differing quite substantially from the IHRG case. Since both the LGPT and the chemical freeze-out are consistently obtained within a single model, their relative location is clarified.

The beam energy dependencies of the skewness and the kurtosis of the baryonic, electric, and strange charge fluctuations have been calculated along the obtained chemical freeze-out curve. All six observables show large deviations from the ideal hadron resonance gas baseline at the highest baryon density at intermediate beam energies. These signals stem in the QvdW-HRG model from the nuclear critical point at $T \sim 20$ MeV and $\mu_B \sim 900$ MeV. This observation must be taken into account in every experimental search for the QCD critical point in high-energy nucleus-nucleus collision experiments using the higher-order fluctuations of conserved charges. This concerns in particular the Beam Energy Scan II run at Brookhaven National Laboratory, as well as future GSI-HADES, FAIR-CBM, and NICA-MPD.

ACKNOWLEDGMENTS

The authors thank M. Gazdzicki, B. I. Lev, and G. M. Zinovjev for fruitful discussions and useful comments. This research was supported by a theme grant of the Department of Physics and Astronomy of NAS of Ukraine: "Dynamics of formation of spatially non-uniform structures in many-body systems," PK 0118U003535. H.S. appreciates the support through the Judah M. Eisenberg Laureatus Chair at Goethe University, and the Walter Greiner Gesellschaft, Frankfurt.

[1] J. Pochodzalla *et al.*, Phys. Rev. Lett. **75**, 1040 (1995).
[2] B. K. Jennings, S. Das Gupta, and N. Mobed, Phys. Rev. C **25**, 278 (1982).
[3] G. Röpke, L. Münchow, and H. Schulz, Nucl. Phys. A **379**, 536 (1982).
[4] G. I. Fai and J. Randrup, Nucl. Phys. A **381**, 557 (1982).
[5] T. Biro, H. W. Barz, B. Lukacs, and J. Zimanyi, Phys. Rev. C **27**, 2695 (1983).
[6] H. Stöcker, A. A. Ogloblin, and W. Greiner, Z. Phys. A: At. Nucl. (1975) **303**, 259 (1981).
[7] L. P. Csernai, H. Stöcker, P. R. Subramanian, G. Buchwald, G. Graebner, A. Rosenhauer, J. A. Maruhn, and W. Greiner, Phys. Rev. C **28**, 2001 (1983).
[8] J. P. Bondorf, R. Donangelo, I. N. Mishustin, C. J. Pethick, H. Schulz, and K. Sneppen, Nucl. Phys. A **443**, 321 (1985).
[9] J. P. Bondorf, R. Donangelo, I. N. Mishustin, and H. Schulz, Nucl. Phys. A **444**, 460 (1985).
[10] J. J. Molitoris, D. Hahn, and H. Stöcker, Nucl. Phys. A **447**, 13C (1986).
[11] D. Hahn and H. Stöcker, Nucl. Phys. A **476**, 718 (1988).
[12] J. Aichelin, G. Peilert, A. Bohnet, A. Rosenhauer, H. Stöcker, and W. Greiner, Phys. Rev. C **37**, 2451 (1988).
[13] G. Peilert, H. Stöcker, W. Greiner, A. Rosenhauer, A. Bohnet, and J. Aichelin, Phys. Rev. C **39**, 1402 (1989).
[14] G. Peilert, J. Randrup, H. Stöcker, and W. Greiner, Phys. Lett. B **260**, 271 (1991).
[15] J. P. Bondorf, A. S. Botvina, A. S. Ilinov, I. N. Mishustin, and K. Sneppen, Phys. Rep. **257**, 133 (1995).
[16] B. Borderie and J. D. Frankland, Prog. Part. Nucl. Phys. **105**, 82 (2019).

[17] M. A. Stephanov, K. Rajagopal, and E. V. Shuryak, Phys. Rev. Lett. **81**, 4816 (1998).
[18] M. A. Stephanov, K. Rajagopal, and E. V. Shuryak, Phys. Rev. D **60**, 114028 (1999).
[19] C. Athanasiou, K. Rajagopal, and M. Stephanov, Phys. Rev. D **82**, 074008 (2010).
[20] M. A. Stephanov, Phys. Rev. Lett. **102**, 032301 (2009).
[21] M. Kitazawa and M. Asakawa, Phys. Rev. C **86**, 024904 (2012); **86**, 069902(E) (2012).
[22] V. Vovchenko, R. V. Poberezhnyuk, D. V. Anchishkin, and M. I. Gorenstein, J. Phys. A: Math. Theor. **49**, 015003 (2016).
[23] V. Vovchenko, D. V. Anchishkin, and M. I. Gorenstein, Phys. Rev. C **91**, 064314 (2015).
[24] R. Poberezhnyuk, V. Vovchenko, M. I. Gorenstein, and H. Stöcker, Phys. Rev. C **99**, 024907 (2019).
[25] V. Vovchenko, D. V. Anchishkin, M. I. Gorenstein, and R. V. Poberezhnyuk, Phys. Rev. C **92**, 054901 (2015).
[26] V. Vovchenko, L. Jiang, M. I. Gorenstein, and H. Stöcker, Phys. Rev. C **98**, 024910 (2018).
[27] V. Vovchenko, M. I. Gorenstein, and H. Stöcker, Phys. Rev. Lett. **118**, 182301 (2017).
[28] V. Vovchenko, D. V. Anchishkin, and M. I. Gorenstein, J. Phys. A: Math. Theor. **48**, 305001 (2015).
[29] K. Redlich and K. Zalewski, Acta Phys. Pol., B **47**, 1943 (2016).
[30] V. Vovchenko, Phys. Rev. C **96**, 015206 (2017).
[31] R. V. Poberezhnyuk, V. Vovchenko, D. V. Anchishkin, and M. I. Gorenstein, Int. J. Mod. Phys. E **26**, 1750061 (2017).
[32] V. Vovchenko and H. Stöcker, Comput. Phys. Commun. **244**, 295 (2019).
[33] C. Patrignani *et al.* (Particle Data Group), Chin. Phys. C **40**, 100001 (2016).
[34] S. Yang, B. N. Zhang, and B. Y. Sun, arXiv:1906.07783.
[35] B. Abelev *et al.* (ALICE Collaboration), Phys. Rev. C **88**, 044910 (2013).
[36] B. B. Abelev *et al.* (ALICE Collaboration), Phys. Rev. Lett. **111**, 222301 (2013).
[37] B. B. Abelev *et al.* (ALICE Collaboration), Phys. Lett. B **728**, 216 (2014); **734**, 409 (2014).
[38] B. B. Abelev *et al.* (ALICE Collaboration), Phys. Rev. C **91**, 024609 (2015).
[39] S. V. Afanasiev *et al.* (NA49 Collaboration), Phys. Rev. C **66**, 054902 (2002).
[40] C. Alt *et al.* (NA49 Collaboration), Phys. Rev. C **73**, 044910 (2006).
[41] C. Alt *et al.* (NA49 Collaboration), Phys. Rev. C **78**, 034918 (2008).
[42] C. Alt *et al.* (NA49 Collaboration), Phys. Rev. C **78**, 044907 (2008).
[43] C. Alt *et al.* (NA49 Collaboration), Phys. Rev. Lett. **94**, 192301 (2005).
[44] T. Anticic *et al.* (NA49 Collaboration), Phys. Rev. C **85**, 044913 (2012).
[45] V. Friese (NA49 Collaboration), Nucl. Phys. A **698**, 487 (2002).
[46] T. Anticic *et al.* (NA49 Collaboration), Phys. Rev. C **84**, 064909 (2011).
[47] C. Alt *et al.* (NA49 Collaboration), Phys. Rev. C **77**, 024903 (2008).
[48] L. Ahle *et al.* (E-802 Collaboration), Phys. Rev. C **59**, 2173 (1999).
[49] L. Ahle *et al.* (E802 Collaboration), Phys. Rev. C **60**, 064901 (1999).
[50] L. Ahle *et al.* (E-802 Collaboration), Phys. Rev. C **60**, 044904 (1999).
[51] F. Becattini, J. Cleymans, A. Keranen, E. Suhonen, and K. Redlich, Phys. Rev. C **64**, 024901 (2001).
[52] J. Cleymans, H. Oeschler, and K. Redlich, Phys. Rev. C **59**, 1663 (1999).
[53] R. Averbeck, R. Holzmann, V. Metag, and R. S. Simon, Phys. Rev. C **67**, 024903 (2003).
[54] P. Braun-Munzinger, J. Cleymans, H. Oeschler, and K. Redlich, Nucl. Phys. A **697**, 902 (2002).
[55] J. Cleymans, B. Hippolyte, H. Oeschler, K. Redlich, and N. Sharma, arXiv:1603.09553.
[56] V. Vovchenko, M. I. Gorenstein, and H. Stöcker, Phys. Rev. C **98**, 034906 (2018).
[57] V. Vovchenko, V. V. Begun, and M. I. Gorenstein, Phys. Rev. C **93**, 064906 (2016).
[58] J. Rafelski, Eur. Phys. J. A **51**, 114 (2015).
[59] F. Becattini, M. Gazdzicki, A. Keranen, J. Manninen, and R. Stock, Phys. Rev. C **69**, 024905 (2004).
[60] V. Vovchenko and H. Stöcker, J. Phys. G **44**, 055103 (2017).
[61] V. Vovchenko and H. Stöcker, Phys. Rev. C **95**, 044904 (2017).
[62] L. M. Satarov, V. Vovchenko, P. Alba, M. I. Gorenstein, and H. Stöcker, Phys. Rev. C **95**, 024902 (2017).
[63] J. Cleymans, H. Oeschler, K. Redlich, and S. Wheaton, Phys. Rev. C **73**, 034905 (2006).
[64] N. U. Bastian, P. Batyuk, D. Blaschke, P. Danielewicz, Yu. B. Ivanov, I. Karpenko, G. Röpke, O. Rogachevsky, and H. H. Wolter, Eur. Phys. J. A **52**, 244 (2016).
[65] G. Röpke, D. Blaschke, Y. B. Ivanov, I. Karpenko, O. V. Rogachevsky, and H. H. Wolter, Phys. Part. Nucl. Lett. **15**, 225 (2018).
[66] J. Randrup and J. Cleymans, Phys. Rev. C **74**, 047901 (2006).
[67] V. V. Begun, M. Gazdzicki, and M. I. Gorenstein, Phys. Rev. C **88**, 024902 (2013).
[68] P. Braun-Munzinger, A. Rustamov, and J. Stachel, Nucl. Phys. A **960**, 114 (2017).
[69] M. I. Gorenstein and M. Gazdzicki, Phys. Rev. C **84**, 014904 (2011).
[70] A. Bzdak and V. Koch, Phys. Rev. C **86**, 044904 (2012).
[71] S. He, X. Luo, Y. Nara, S. Esumi, and N. Xu, Phys. Lett. B **762**, 296 (2016).
[72] Y. Ye, Y. Wang, J. Steinheimer, Y. Nara, H.-j. Xu, P. Li, D. Lu, Q. Li, and H. Stöcker, Phys. Rev. C **98**, 054620 (2018).